

Measurement of χ_{cJ} Decays to $2(\pi^+\pi^-)p\bar{p}$ Final States

M. Ablikim¹, J. Z. Bai¹, Y. Ban¹², J. G. Bian¹, X. Cai¹, H. F. Chen¹⁷, H. S. Chen¹, H. X. Chen¹, J. C. Chen¹, Jin Chen¹, Y. B. Chen¹, S. P. Chi², Y. P. Chu¹, X. Z. Cui¹, Y. S. Dai¹⁹, L. Y. Diao⁹, Z. Y. Deng¹, Q. F. Dong¹⁵, S. X. Du¹, J. Fang¹, S. S. Fang², C. D. Fu¹, C. S. Gao¹, Y. N. Gao¹⁵, S. D. Gu¹, Y. T. Gu⁴, Y. N. Guo¹, Y. Q. Guo¹, Z. J. Guo¹⁶, F. A. Harris¹⁶, K. L. He¹, M. He¹³, Y. K. Heng¹, H. M. Hu¹, T. Hu¹, G. S. Huang¹⁶, X. T. Huang¹³, X. B. Ji¹, X. S. Jiang¹, X. Y. Jiang⁵, J. B. Jiao¹³, D. P. Jin¹, S. Jin¹, Yi Jin⁸, Y. F. Lai¹, G. Li², H. B. Li¹, H. H. Li¹, J. Li¹, R. Y. Li¹, S. M. Li¹, W. D. Li¹, W. G. Li¹, X. L. Li¹, X. N. Li¹, X. Q. Li¹¹, Y. L. Li⁴, Y. F. Liang¹⁴, H. B. Liao⁶, B. J. Liu¹, C. X. Liu¹, F. Liu⁶, Fang Liu¹, H. H. Liu¹, H. M. Liu¹, J. Liu¹², J. B. Liu¹, J. P. Liu¹⁸, Q. Liu¹, R. G. Liu¹, Z. A. Liu¹, Y. C. Lou⁵, F. Lu¹, G. R. Lu⁵, J. G. Lu¹, C. L. Luo¹⁰, F. C. Ma⁹, H. L. Ma¹, L. L. Ma¹, Q. M. Ma¹, X. B. Ma⁵, Z. P. Mao¹, X. H. Mo¹, J. Nie¹, S. L. Olsen¹⁶, H. P. Peng^{17f}, R. G. Ping¹, N. D. Qi¹, H. Qin¹, J. F. Qiu¹, Z. Y. Ren¹, G. Rong¹, L. Y. Shan¹, L. Shang¹, C. P. Shen¹, D. L. Shen¹, X. Y. Shen¹, H. Y. Sheng¹, H. S. Sun¹, J. F. Sun¹, S. S. Sun¹, Y. Z. Sun¹, Z. J. Sun¹, Z. Q. Tan⁴, X. Tang¹, G. L. Tong¹, G. S. Varner¹⁶, D. Y. Wang¹, L. Wang¹, L. L. Wang¹, L. S. Wang¹, M. Wang¹, P. Wang¹, P. L. Wang¹, W. F. Wang^{1d}, Y. F. Wang¹, Z. Wang¹, Z. Y. Wang¹, Zhe Wang¹, Zheng Wang², C. L. Wei¹, D. H. Wei¹, N. Wu¹, X. M. Xia¹, X. X. Xie¹, G. F. Xu¹, Y. Xu¹¹, M. L. Yan¹⁷, H. X. Yang¹, Y. X. Yang³, M. H. Ye², Y. X. Ye¹⁷, Z. Y. Yi¹, G. W. Yu¹, C. Z. Yuan¹, J. M. Yuan¹, Y. Yuan¹, S. L. Zang¹, Y. Zeng⁷, Yu Zeng¹, B. X. Zhang¹, B. Y. Zhang¹, C. C. Zhang¹, D. H. Zhang¹, H. Q. Zhang¹, H. Y. Zhang¹, J. W. Zhang¹, J. Y. Zhang¹, S. H. Zhang¹, X. M. Zhang¹, X. Y. Zhang¹³, Yiyun Zhang¹⁴, Z. P. Zhang¹⁷, D. X. Zhao¹, J. W. Zhao¹, M. G. Zhao¹, P. P. Zhao¹, W. R. Zhao¹, Z. G. Zhao^{1e}, H. Q. Zheng¹², J. P. Zheng¹, Z. P. Zheng¹, L. Zhou¹, N. F. Zhou^{1e}, K. J. Zhu¹, Q. M. Zhu¹, Y. C. Zhu¹, Y. S. Zhu¹, Yingchun Zhu^{1f}, Z. A. Zhu¹, B. A. Zhuang¹, X. A. Zhuang¹, B. S. Zou¹

(BES Collaboration)

¹ *Institute of High Energy Physics, Beijing 100049, People's Republic of China*

² *China Center for Advanced Science and Technology (CCAST), Beijing 100080, People's Republic of China*

³ *Guangxi Normal University, Guilin 541004, People's Republic of China*

⁴ *Guangxi University, Nanning 530004, People's Republic of China*

⁵ *Henan Normal University, Xinxiang 453002, People's Republic of China*

⁶ *Huazhong Normal University, Wuhan 430079, People's Republic of China*

⁷ *Hunan University, Changsha 410082, People's Republic of China*

⁸ *Jinan University, Jinan 250022, People's Republic of China*

⁹ *Liaoning University, Shenyang 110036, People's Republic of China*

¹⁰ *Nanjing Normal University, Nanjing 210097, People's Republic of China*

¹¹ *Nankai University, Tianjin 300071, People's Republic of China*

¹² *Peking University, Beijing 100871, People's Republic of China*

¹³ *Shandong University, Jinan 250100, People's Republic of China*

¹⁴ *Sichuan University, Chengdu 610064, People's Republic of China*

¹⁵ *Tsinghua University, Beijing 100084, People's Republic of China*

¹⁶ *University of Hawaii, Honolulu, HI 96822, USA*

¹⁷ *University of Science and Technology of China, Hefei 230026, People's Republic of China*

¹⁸ *Wuhan University, Wuhan 430072, People's Republic of China*

¹⁹ *Zhejiang University, Hangzhou 310028, People's Republic of China*

^a *Current address: Iowa State University, Ames, IA 50011-3160, USA*

^b *Current address: Purdue University, West Lafayette, IN 47907, USA*

^c *Current address: Cornell University, Ithaca, NY 14853, USA*

^d *Current address: Laboratoire de l'Accélérateur Linéaire, Orsay, F-91898, France*

^e *Current address: University of Michigan, Ann Arbor, MI 48109, USA*

^f *Current address: DESY, D-22607, Hamburg, Germany*

Using $\chi_{cJ} \rightarrow 2(\pi^+\pi^-)p\bar{p}$ decays from 14×10^6 $\psi(2S)$ events accumulated by the BESII detector at the BEPC, the intermediate states $\Xi^-\bar{\Xi}^+$, $\Lambda\bar{\Lambda}\pi^+\pi^-$, and $K_S^0 K_S^0 p\bar{p}$ are studied, and their branching ratios or upper limits are measured.

PACS numbers: 12.38.Qk, 13.20.Gd, 13.25.Gv, 13.40.Hq

I. INTRODUCTION

Experimental studies on charmonia decay properties are essential to test perturbative QCD models and QCD based calculations. The importance of the Color Octet Mechanism (COM) for χ_{cJ} decays has been pointed out for many years [1], and theoretical predictions of two-body exclusive decays have been made based on it. Recently, new experimental results on χ_{cJ} exclusive decays have been reported [2, 3]. COM predictions for many χ_{cJ} decays into meson pairs are in agreement with experimental values, while predictions for some decays into baryon pairs, for example, the branching fractions of $\chi_{cJ} \rightarrow \Lambda\bar{\Lambda}$, disagree with measured values. For further testing of the COM in the decays of the P-wave charmonia, measurements of other baryon pair decays of χ_{cJ} , such as $\chi_{cJ} \rightarrow \Xi^-\bar{\Xi}^+$ and $\Sigma^0\bar{\Sigma}^0$ are desired.

The measurement of $\chi_{c0} \rightarrow \Xi^-\bar{\Xi}^+$ is helpful for understanding the Helicity Selection Rule (HSR) [4], which prohibits χ_{c0} decays into baryon antibaryon ($B\bar{B}$) pairs. However, the measured branching ratios for χ_{c0} decays into $p\bar{p}$ and $\Lambda\bar{\Lambda}$ do not vanish, demonstrating a strong violation of HSR in charmonium decays. Measurements of χ_{c0} decays into other baryon anti-baryon pairs would provide additional tests of the HSR.

In this paper, the analysis of $\psi(2S) \rightarrow \gamma 2(\pi^+\pi^-)p\bar{p}$ decays using 14×10^6 $\psi(2S)$ events collected at BE-SII/BEPC is reported. We observe $\chi_{cJ} \rightarrow \Xi^-\bar{\Xi}^+$ and $\Lambda\bar{\Lambda}\pi^+\pi^-$ decays and search for $\chi_{cJ} \rightarrow K_S^0 K_S^0 p\bar{p}$; results are compared with theoretical predictions.

II. BES DETECTOR

This analysis is based on a sample of 14×10^6 $\psi(2S)$ events taken with the BESII detector at the BEPC storage ring at a center-of-mass energy of $M_{\psi(2S)}$ with an integrated luminosity of $19.72 \pm 0.86 \text{ pb}^{-1}$ [5]. BES is a conventional solenoidal magnet detector that is described in detail in Ref. [6]; BESII is the upgraded version [7]. A 12-layer vertex chamber (VC) surrounding the beam pipe provides trigger and trajectory information. A forty-layer main drift chamber (MDC), located radially outside the VC, provides trajectory and energy loss (dE/dx) information for charged tracks over 85% of the total solid angle. The momentum resolution is $\sigma_p/p = 0.017\sqrt{1+p^2}$ (p in GeV/c), and the dE/dx resolution for hadron tracks is $\sim 8\%$. An array of 48 scintillation counters surrounding the MDC measures the time-of-flight (TOF) of charged tracks with a resolution of ~ 200 ps for hadrons. Radially outside the TOF system is a 12 radiation length, lead-gas barrel shower counter (BSC). This measures the energies of electrons and photons over $\sim 80\%$ of the solid angle with an energy resolution of $\sigma_E/E = 22\%/\sqrt{E}$ (E in GeV). Outside of the solenoidal coil, which provides a 0.4 Tesla magnetic field over the tracking volume, is the iron flux return which is instrumented with three double layers of counters that identify muons with momentum greater than 0.5 GeV/c.

III. MONTE-CARLO SIMULATION

A GEANT3 based Monte Carlo simulation program, SIMBES [8], which simulates the detector response, including interactions of secondary particles in the detector materials, is used to determine detection efficiencies and mass resolutions, as well as to optimize selection criteria and estimate backgrounds. Under the assumption of a pure E1 transition, the distribution of polar angle θ of the outgoing photon in $\psi(2S) \rightarrow \gamma\chi_{cJ}$ decays is given by $1 + \alpha\cos^2\theta$ with $\alpha = 1, -1/3, \text{ and } 1/13$ for $J = 0, 1, \text{ and } 2$, respectively [9]. Angular distributions of daughter particles for the sequential decays $\chi_{cJ} \rightarrow \Xi^-\bar{\Xi}^+, \Xi \rightarrow \Lambda\pi$ are simulated based on the transitional amplitude information method [10]. Angular distributions of daughter particles from the other multi-body decays are generated isotropically in the center-of-mass of $\psi(2S)$ or χ_{cJ} .

IV. EVENT SELECTION

The selection criteria described below are similar to those used in previous BES analyses [2].

A. Photon identification

A shower cluster in the BSC is considered to be a photon candidate, if it has an energy deposit of more than 50 MeV, the angle between the nearest charged track and the cluster is greater than 12° , the first hit is in the

beginning six radiation lengths, and the difference between the angle of the cluster development direction in the BSC and the photon emission direction is less than 37° .

B. Charged particle identification

Each charged track is required to have a good helix fit and a polar angle θ that satisfies $|\cos\theta| < 0.8$. The TOF and dE/dx measurements of the charged track are used to calculate χ_{PID}^2 values and the corresponding confidence levels for the hypotheses that the particle is a pion, kaon, or proton.

C. Event selection criteria

Candidate events are required to satisfy the following selection criteria:

1. The number of charged tracks is required to be six with net charge zero, and the number of photon candidates must be less than four.
2. The proton and antiproton must be identified using particle identification; their particle identification confidence levels must be greater than 1%.
3. Four-constraint (4-C) kinematic fits to the $\psi(2S) \rightarrow \gamma 2(\pi^+\pi^-)p\bar{p}$ hypothesis are performed using each photon candidate. The combination with the minimum combined $\chi_{comb}^2 = \sum_i^{n_{chrg}} (\chi_{dE/dx}^2 + \chi_{TOF}^2)_i + \chi_{4C}^2$ is selected, and the 4-C fit confidence level for the selected combination must be greater than 1%.
4. To remove the background channels: $\psi(2S) \rightarrow \gamma 2(\pi^+\pi^-)K^+K^-$, $\gamma 3(\pi^+\pi^-)$, and $2(\pi^+\pi^-)p\bar{p}$, χ_{comb}^2 of the signal channel is required to be less than those of the background channels, i.e., $\chi_{comb}^2(signal) < \chi_{comb}^2(bg)$.

V. DATA ANALYSIS

A. $\chi_{cJ} \rightarrow \Xi^-\bar{\Xi}^+$

The sequential decays $\Xi \rightarrow \Lambda\pi, \Lambda \rightarrow p\pi$ are used to reconstruct $\chi_{cJ} \rightarrow \Xi^-\bar{\Xi}^+$. The $p\pi^-$ invariant mass distribution for candidate events is shown in Figure 1(a), where a clear Λ signal is seen. A $\bar{\Lambda}$ signal appears similarly in the $\bar{p}\pi^+$ invariant mass distribution. The Λ mass resolution, obtained from MC simulation, is $5.5 \text{ MeV}/c^2$. After requiring that Λ and $\bar{\Lambda}$ satisfy $|m_\Lambda - m_{p\pi^-}| < 11 \text{ MeV}/c^2$ (2σ), the scatter plot of $m_{\Lambda\pi^-}$ versus $m_{\bar{\Lambda}\pi^+}$ is given in Figure 1(b). In Figure 1(c), the $m_{\Lambda\pi^-}$ distribution is shown after the requirement $|m_{\bar{\Lambda}\pi^+} - m_\Xi| < 17.5 \text{ MeV}/c^2$ (2σ), where the Ξ^- appears clearly. After requiring that $\Lambda\pi^-$ and $\bar{\Lambda}\pi^+$ satisfy $|M_{\Lambda\pi^-} - M_\Xi| < 17.5 \text{ MeV}/c^2$, the $m_{\Xi^-\bar{\Xi}^+}$ distribution is plotted in Figure 1(d), and the normalized background distribution determined from the $\Lambda\bar{\Lambda}$ sideband region is also shown in the plot.

To determine the detection efficiencies, the angular distributions of the decay particles for the sequential decays $\psi(2S) \rightarrow \gamma\chi_{cJ}, \chi_{cJ} \rightarrow \Xi^-\bar{\Xi}^+, \Xi \rightarrow \Lambda\pi, \Lambda \rightarrow p\pi$ are simulated based on the transitional amplitude information (TAI) method [10]. The detection efficiencies are $(2.3 \pm 0.1)\%$, $(2.6 \pm 0.1)\%$, and $(2.3 \pm 0.1)\%$ for $\psi(2S)$ sequential decays to $\Xi^-\bar{\Xi}^+$ via χ_{c0}, χ_{c1} , and χ_{c2} , respectively.

The main backgrounds from channels with Ξ or Λ production, including $\psi(2S) \rightarrow \Xi^-\bar{\Xi}^+, \psi(2S) \rightarrow \gamma\chi_{cJ} \rightarrow \gamma\Sigma(1385)\bar{\Sigma}(1385), \psi(2S) \rightarrow \gamma\chi_{cJ} \rightarrow \gamma\Sigma^0\bar{\Sigma}^0$, and $\psi(2S) \rightarrow \gamma\chi_{cJ} \rightarrow \gamma\Xi^0\bar{\Xi}^0$ are determined by Monte-Carlo simulation. By using the branching ratio of $\psi(2S) \rightarrow \Xi^-\bar{\Xi}^+$ measured in [11] and naively assuming $\chi_{cJ} \rightarrow \Sigma(1385)\bar{\Sigma}(1385), \Sigma^0\bar{\Sigma}^0, \Xi^0\bar{\Xi}^0$ have the same branching ratio as $\chi_{cJ} \rightarrow \Lambda\bar{\Lambda}$, one obtains 0.03, 0.01, and 0.02 background events for χ_{c0}, χ_{c1} , and χ_{c2} , respectively.

Figure 2 shows the fit to the $m_{\Xi^-\bar{\Xi}^+}$ distribution using a signal shape obtained from MC simulation. One obtains 6.4 ± 3.2 events for $\chi_{c0} \rightarrow \Xi^-\bar{\Xi}^+$. Within twice the mass resolution of the χ_{c1} and χ_{c2} , one event is respectively observed. Upper limits at the 90% Confidence Level (CL) for $\chi_{c1} \rightarrow \Xi^-\bar{\Xi}^+$ and $\chi_{c2} \rightarrow \Xi^-\bar{\Xi}^+$ are evaluated with POLE [12] including systematic uncertainties, and the results are listed in Table I. The branching ratios and upper limits ($N^{sig} \rightarrow N_{upper}$) are estimated with:

$$B[\chi_{cJ} \rightarrow \Xi^-\bar{\Xi}^+] = \frac{N^{sig}/\epsilon}{N_{\psi(2S)}B[\psi(2S) \rightarrow \gamma\chi_{cJ}]B[\Xi \rightarrow \pi\Lambda]^2B[\Lambda \rightarrow p\pi]^2}, \quad (1)$$

where ϵ denotes the detection efficiency and $N^{sig} = N^{obs} - N^{bg}$ denotes the number of signal events observed.

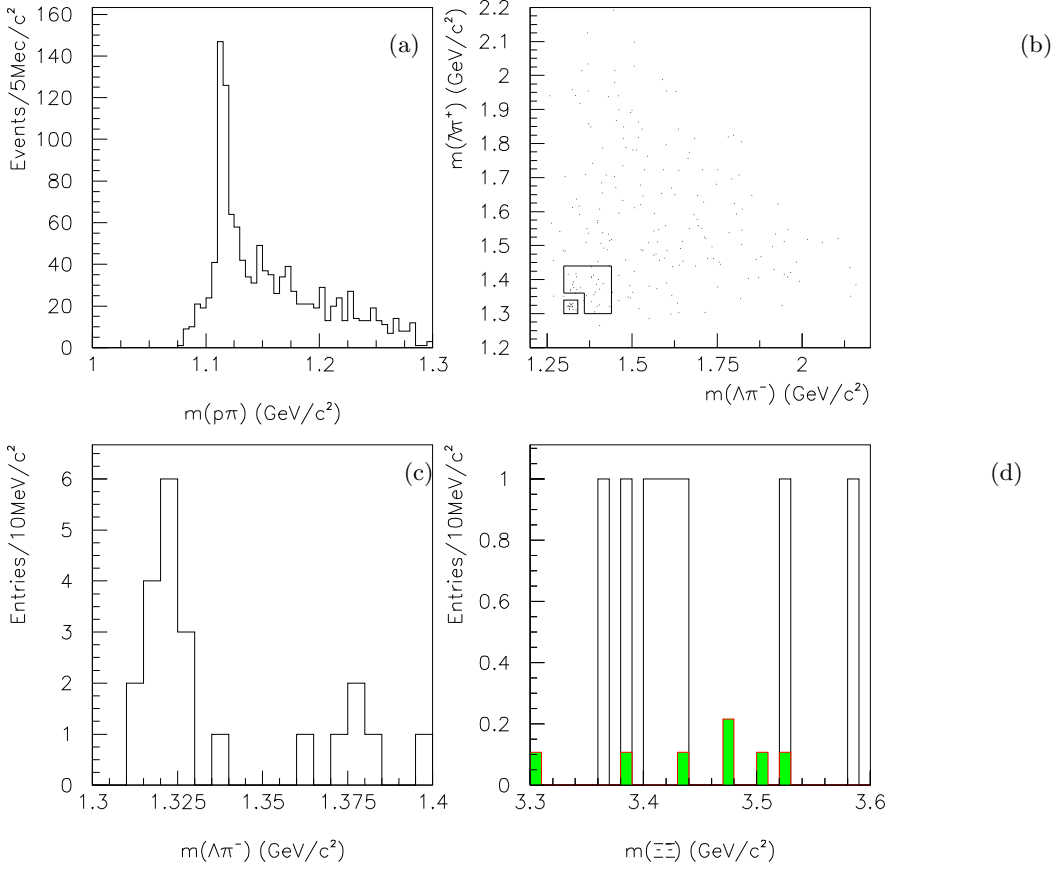


Fig. 1: (a) The $p\pi$ invariant mass distribution. (b) Scatter plot of $m_{\Lambda\pi^-}$ versus $m_{\Lambda\pi^+}$, where the small square corresponds to the $\Xi^- \bar{\Xi}^+$ signal region and the larger closed area to the $\Xi^- \bar{\Xi}^+$ sideband region. (c) $\Lambda\pi^-$ mass distribution for $|m_{\Lambda\pi^+} - m_{\Xi}| < 17.5$ MeV/c². (d) The $m_{\Xi^- \bar{\Xi}^+}$ invariant mass distribution, where the shaded histogram corresponds to the contribution from the $\Xi^- \bar{\Xi}^+$ sideband region (normalized).

TABLE I: Summary of numbers used in the branching ratio calculation, where the branching ratio for $\psi(2S) \rightarrow \gamma\chi_{cJ}$ are taken from Ref. [13]

quantity	χ_{c0}	χ_{c1}	χ_{c2}
N^{obs}	6.4 ± 3.2	1.0	1.0
N_{upper}	12.4	4.6	4.6
ϵ (%)	2.3 ± 0.1	2.6 ± 0.1	2.3 ± 0.1
$N_{\psi(2S)} (\times 10^6)$	14.0 ± 0.6	14.0 ± 0.6	14.0 ± 0.6
$B(\psi(2S) \rightarrow \gamma\chi_{cJ})$ (%)	9.2 ± 0.5	9.1 ± 0.6	9.3 ± 0.6
$B(\Xi \rightarrow \Lambda\pi)$ (%)	99.9 ± 0.1	99.9 ± 0.1	99.9 ± 0.1
$B(\Lambda \rightarrow p\pi)$ (%)	63.9 ± 0.5	63.9 ± 0.5	63.9 ± 0.5
$B(\chi_{cJ} \rightarrow \Xi^- \bar{\Xi}^+) \times 10^{-4}$	$5.3 \pm 2.7 \pm 0.9$	< 3.4 (90% C.L.)	< 3.7 (90% C.L.)
	< 10.3 (90% C.L.)		

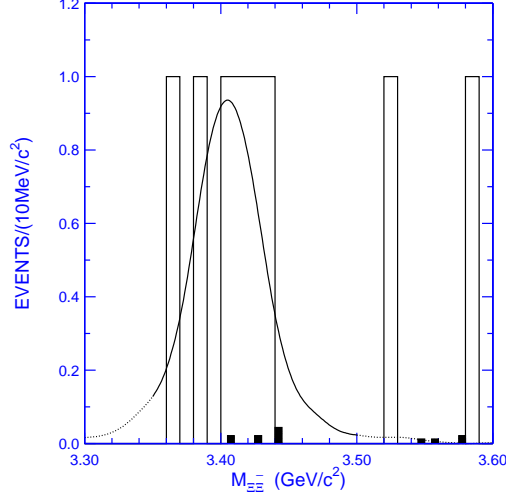


Fig. 2: Fit to the $\Xi^-\bar{\Xi}^+$ mass spectrum for $\chi_{c0} \rightarrow \Xi^-\bar{\Xi}^+$ with the signal shape obtained from Monte-Carlo simulation. The histogram corresponds to the data, and the shaded histogram to the normalized backgrounds obtained from Monte-Carlo simulation.

B. $\chi_{cJ} \rightarrow \Lambda\bar{\Lambda}\pi^+\pi^-$

The Λ and $\bar{\Lambda}$ candidates are reconstructed the same as in the above analysis. The $\chi_{cJ} \rightarrow \Xi^-\bar{\Xi}^+$ candidates are excluded. Figure 3(a) shows the scatter plot of $m_{p\pi^-}$ versus $m_{\bar{p}\pi^+}$ for candidate events. The dense cluster in the square, with side twice the Λ mass resolution, corresponds to the $\Lambda\bar{\Lambda}$ signal. The $\Lambda\bar{\Lambda}$ sideband region is shown in the same plot. Figure 3(b) shows the distribution of $m_{\Lambda\bar{\Lambda}\pi^+\pi^-}$ (full histogram) and $\Lambda\bar{\Lambda}$ sideband background (shaded histogram).

To determine the detection efficiency, sequential decays via $\chi_{cJ} \rightarrow \Lambda\bar{\Lambda}\pi^+\pi^-$, $\Lambda \rightarrow p\pi$ are simulated assuming a pure phase space distribution. After applying the same selection criteria, one obtains detection efficiencies of $(0.93 \pm 0.04)\%$, $(1.14 \pm 0.04)\%$, and $(1.11 \pm 0.04)\%$ for χ_{c0} , χ_{c1} , and χ_{c2} decays, respectively. The decrease in detection efficiency, compared with the two-body sequential decay via $\chi_{cJ} \rightarrow \Xi^-\bar{\Xi}^+$, is due to the difference in the momentum distributions of the decay particles in $\chi_{cJ} \rightarrow \Lambda\bar{\Lambda}\pi^+\pi^-$.

Potential background contaminations, including $\psi(2S) \rightarrow \gamma\chi_{cJ} \rightarrow \gamma\rho^0\Delta^{++}\Delta^{--} \rightarrow \gamma 2(\pi^+\pi^-)p\bar{p}$, $\psi(2S) \rightarrow \pi^+\pi^-J/\psi$, then $J/\psi \rightarrow \gamma\eta_c \rightarrow \gamma p\pi^+\bar{\Delta}^{--}$, $\gamma\rho^0 p\bar{p}$, and $J/\psi \rightarrow \eta p\bar{p} \rightarrow \gamma\pi^+\pi^-p\bar{p}$, are studied by Monte-Carlo simulation, and it is found that these background contaminations are effectively removed by the $\Lambda\bar{\Lambda}$ sideband background subtraction.

Figure 4 shows the $m_{\Lambda\bar{\Lambda}\pi^+\pi^-}$ distribution after subtracting the $\Lambda\bar{\Lambda}$ sideband background. Breit-Wigner functions, convoluted with Gaussian mass resolutions, for the χ_{c0} , χ_{c1} , and χ_{c2} resonances and a polynomial background shape are used to fit the $m_{\Lambda\bar{\Lambda}\pi^+\pi^-}$ distribution from 3.3 to 3.65 GeV/c^2 . The number of signal events obtained are $n^{sig} = 9.6 \pm 5.4$, 0.2 ± 3.2 , and 10.4 ± 5.7 for χ_{c0} , χ_{c1} , and χ_{c2} , respectively. The upper limits at the 90% C.L. are estimated with POLE including systematic uncertainties and also listed in Table II.

TABLE II: Summary of numbers used in the branching ratio calculation for $\chi_{cJ} \rightarrow \Lambda\bar{\Lambda}\pi^+\pi^-$.

quantity	χ_{c0}	χ_{c1}	χ_{c2}
n^{sig}	9.6 ± 5.4	—	10.4 ± 5.7
N_{upper}	19.6	8.8	20.4
$\epsilon (\times 10^{-3})$	9.3 ± 0.4	11.4 ± 0.4	11.1 ± 0.4
$N_{\psi(2S)} (\times 10^6)$	14 ± 0.6	14 ± 0.6	14 ± 0.6
$B(\psi(2S) \rightarrow \gamma\chi_{cJ}) (\%)$	9.2 ± 0.5	9.1 ± 0.6	9.3 ± 0.6
$B(\Lambda \rightarrow p\pi) (\%)$	63.9 ± 0.5	63.9 ± 0.5	63.9 ± 0.5
$B(\chi_{cJ} \rightarrow \pi^+\pi^-\Lambda) \times 10^{-3}$	$2.0 \pm 1.1 \pm 0.4 (2.5\sigma)$	—	$1.8 \pm 1.0 \pm 0.3 (2.5\sigma)$
upper-limit $\times 10^{-3}$ (90% C.L.)	< 4.0	< 1.5	< 3.5

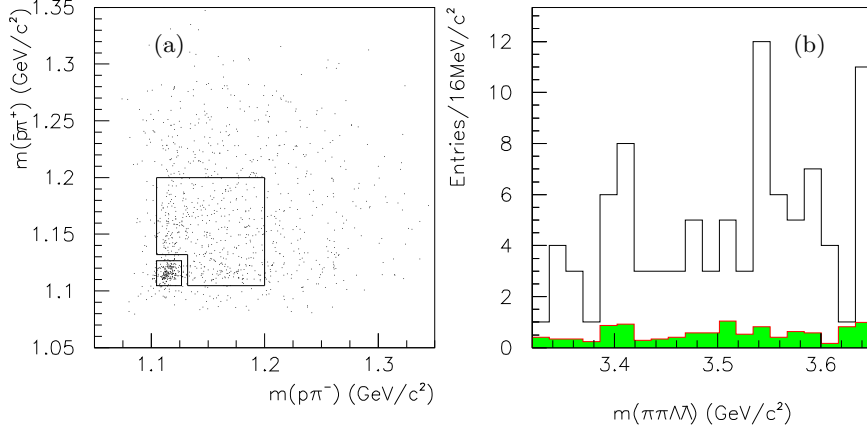


Fig. 3: (a) Scatter plot of $m_{p\pi^-}$ versus $m_{\bar{p}\pi^+}$ for candidate events, where the square box corresponds to the $\Lambda\bar{\Lambda}$ signal region, and the large box beside it corresponds to the $\Lambda\bar{\Lambda}$ sideband region. (b) The $m_{\Lambda\bar{\Lambda}\pi\pi}$ invariant mass distribution of events in the $\Lambda\bar{\Lambda}$ region (full histogram) and normalized $\Lambda\bar{\Lambda}$ sideband background (shaded histogram).

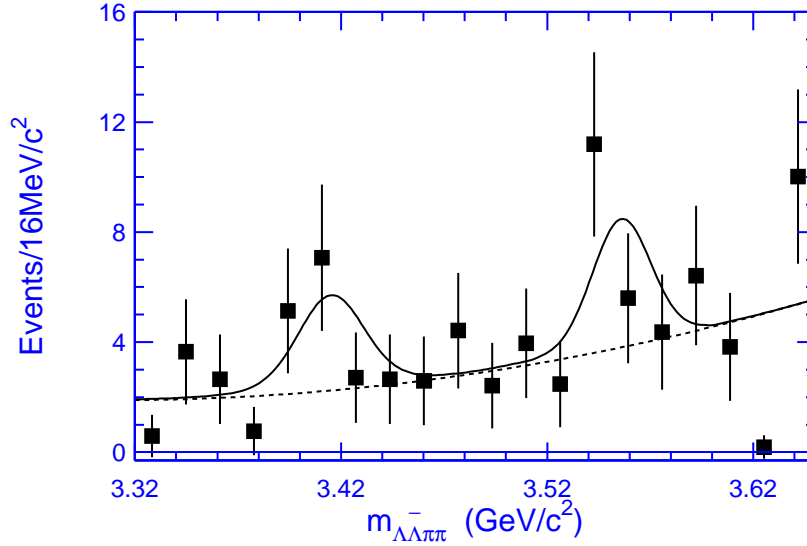


Fig. 4: Fit to the $m_{\Lambda\bar{\Lambda}\pi^+\pi^-}$ distribution after subtracting $\Lambda\bar{\Lambda}$ sideband background. The squares with error bars are data, the dashed curve is a second order polynomial to represent background, and the solid curve is the fit.

The branching ratios and upper limits ($N^{sig} \rightarrow N_{upper}$) are estimated using:

$$B[\chi_{cJ} \rightarrow \Lambda\bar{\Lambda}\pi^+\pi^-] = \frac{N^{sig}/\epsilon}{N_{\psi(2S)}B[\psi(2S) \rightarrow \gamma\chi_{cJ}]B[\Lambda \rightarrow p\pi]^2}, \quad (2)$$

where n^{sig} denotes the number of signal events. The branching ratios and upper limits are listed in Table II.

C. $\chi_{cJ} \rightarrow K_S^0 K_S^0 p\bar{p}$

K_S^0 candidates are selected by choosing the $\pi^+\pi^-$ combinations with the minimum value of $\Delta(i_1, i_2, j_1, j_2) = (m_{\pi^+(i_1)\pi^-(j_1)} - m_{K_S^0})^2 + (m_{\pi^+(i_2)\pi^-(j_2)} - m_{K_S^0})^2$ and requiring the K_S^0 candidates to satisfy $|M_{K_S^0} - M_{\pi^+\pi^-}| < 15 \text{ MeV}/c^2$ (2σ). The candidates for $\chi_{cJ} \rightarrow \Lambda\bar{\Lambda}\pi^+\pi^-$ are excluded.

The scatter plot of $m_{\pi^+\pi^-}$ versus $m_{\pi^+\pi^-}$ is shown in Figure 5(a), where the events in the central square are $K_S^0 K_S^0$ signal candidates and the four surrounding squares are the $K_S^0 K_S^0$ sideband regions. Figure 5(b) shows the $m_{\pi\pi}$ invariant mass distribution. In the K_S^0 mass region, no significant signal is observed. After applying the selection criteria for $K_S^0 K_S^0$, the distribution of $m_{K_S^0 K_S^0 p\bar{p}}$ is given in Figure 5(c). Within selection regions which are twice the χ_{cJ} mass resolution, the observed numbers of events are 2, 0, and 2 for χ_{c0} , χ_{c1} , and χ_{c2} , respectively. Figure 5(d) shows the background from the $K_S^0 K_S^0$ sideband background region. The K_S^0 sideband regions are defined as $445.1 \text{ MeV}/c^2 < m_{\pi^+\pi^-} < 475.1 \text{ MeV}/c^2$ and $520.1 \text{ MeV}/c^2 < m_{\pi^+\pi^-} < 550.1 \text{ MeV}/c^2$, and the mass of other two pions is required to satisfy $|M_{K_S^0} - M_{\pi^+\pi^-}| < 15 \text{ MeV}/c^2$. The numbers of background events observed are 1.3, 1.5, and 0.5 for χ_{c0} , χ_{c1} , and χ_{c2} respectively. The upper limits at the 90% C.L. are estimated with POLE including systematic uncertainties, and the results are listed in Table III.

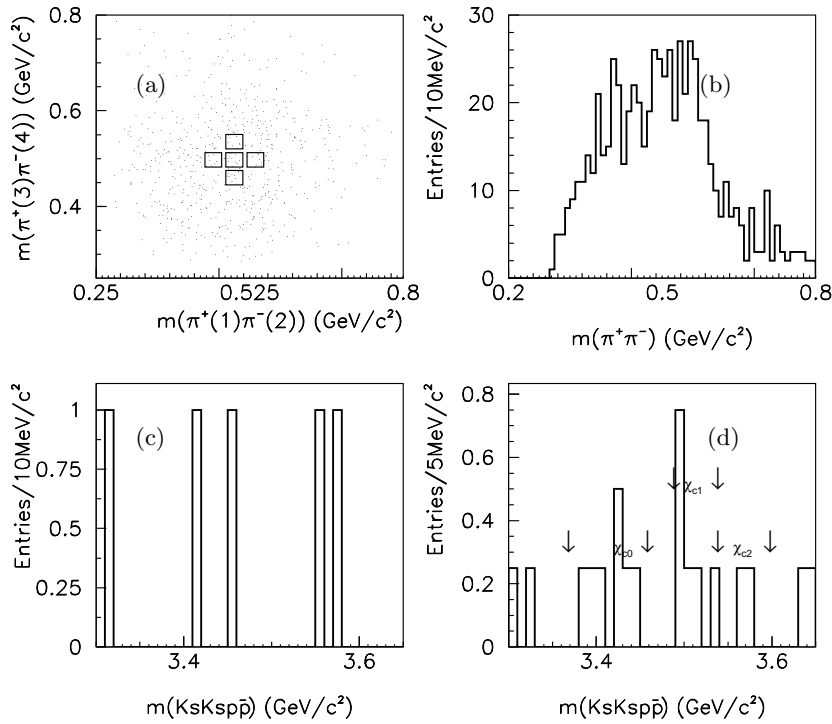


Fig. 5: (a) The scatter plot of $m_{\pi^+\pi^-}$ versus $m_{\pi^+\pi^-}$. (b) The $m_{\pi^+\pi^-}$ invariant mass distribution. (c) The $m_{K_S^0 K_S^0 p\bar{p}}$ invariant mass distribution. (d) The $m_{K_S^0 K_S^0 p\bar{p}}$ invariant mass distribution (normalized) for events in the $K_S^0 K_S^0$ sideband regions.

The detection efficiencies are $(0.87 \pm 0.06)\%$, $(0.92 \pm 0.06)\%$, and $(0.90 \pm 0.06)\%$ for χ_{c0} , χ_{c1} , and χ_{c2} decays, respectively. Upper limits are estimated using

$$B[\chi_{cJ} \rightarrow K_S^0 K_S^0 p\bar{p}] = \frac{N_{upper}/\epsilon}{N_{\psi(2S)} B[\psi(2S) \rightarrow \gamma \chi_{cJ}] B[K_S^0 \rightarrow \pi^+\pi^-]^2}, \quad (3)$$

where ϵ denotes the detection efficiency. The upper limits for $\chi_{cJ} \rightarrow K_S^0 K_S^0 p\bar{p}$ are listed in Table III.

TABLE III: Summary of numbers used in the branching ratios calculation of $\chi_{cJ} \rightarrow K_S^0 K_S^0 p \bar{p}$.

quantity	χ_{c0}	χ_{c1}	χ_{c2}
n_{upper}	4.7	2.5	4.4
$\epsilon (\times 10^{-3})$	8.7 ± 0.6	9.2 ± 0.6	9.0 ± 0.6
$N_{\psi(2S)} (\times 10^6)$	14.0 ± 0.6	14.0 ± 0.6	14.0 ± 0.6
$B(\psi(2S) \rightarrow \gamma \chi_{cJ}) (\%)$	9.2 ± 0.5	9.1 ± 0.6	9.3 ± 0.6
$B(K_S^0 \rightarrow \pi^+ \pi^-) (\%)$	69.0 ± 0.1	69.0 ± 0.1	69.0 ± 0.1
$B(\chi_{cJ} \rightarrow K_S^0 K_S^0 p \bar{p}) \times 10^{-4}$			
upper-limit (90% C.L.)	< 8.8	< 4.5	< 7.9

VI. SYSTEMATIC ERRORS

Systematic errors on the branching fractions mainly originate from the MC statistics, the track error matrix, the kinematic fit, particle identification, the photon efficiency, the uncertainty of the branching fractions of the intermediate states (from PDG or published papers), the total number of $\psi(2S)$ events, the fitting, the uncertainty of the angular distribution of the Ξ in χ_{cJ} decays, and efficiency corrections from $\chi_{cJ} \rightarrow \Sigma^-(1385)\bar{\Lambda}\pi^+ + c.c.$

- As studied by a previous BES analysis [14] using clean channels like $J/\psi \rightarrow \Lambda\bar{\Lambda}$ and $\psi' \rightarrow \pi^+\pi^-J/\psi \rightarrow \pi^+\pi^-\mu^+\mu^-$, it is found that the tracking efficiency for MC simulation agrees with data within (1-2)% for each charged track. Hence, we take 12% as the systematic error for events with six charged tracks.
- The photon detection efficiency was studied using different methods with $J/\psi \rightarrow \pi^+\pi^-\pi^0$ events [15], and the difference between data and MC simulation is about 2% for each photon. We take 2% as the systematic error for decays with one photon.
- A kinematic fit is applied to the channels analyzed, and a probability > 0.01 is required. The consistency between data and Monte Carlo efficiencies for the kinematic fit depends on whether the track fitting error matrices are consistent for data and MC simulation. From earlier studies, we take 4% as the systematic error for kinematic fitting [16].
- The p and \bar{p} candidates are identified with the requirement that the particle identification confidence level be greater than 0.01. Comparing data and MC data samples for the decay $\psi(2S) \rightarrow \pi^+\pi^-J/\psi, J/\psi \rightarrow \pi^0 p \bar{p}$, the efficiency difference is about 2.8% for one particle identified as a proton or antiproton. Here 5.6% is taken as the systematic error for $p\bar{p}$ identification.
- To estimate the background uncertainty for $\chi_{cJ} \rightarrow \Xi^-\bar{\Xi}^+$, background MC samples and $\Xi^-\bar{\Xi}^+$ sideband backgrounds are used. The maximum difference between them is about 5%, which is taken as the systematic error. For $\chi_{cJ} \rightarrow \Lambda\bar{\Lambda}\pi^+\pi^-$, the background uncertainty includes the uncertainty in the background shape and fitting interval; the differences found using different shapes and intervals are 5.25%, 3.57%, and 2.85% for χ_{c0}, χ_{c1} , and χ_{c2} decays, respectively. For $\chi_{cJ} \rightarrow K_S^0 K_S^0 p \bar{p}$ decays, the maximum difference in estimation of the upper limits between different choices of $K_S^0 K_S^0$ sideband regions is about 4%, which is taken as the systematic error.
- To determine the detection efficiency for $\chi_{cJ} \rightarrow \Xi^-\bar{\Xi}^+$, the TAI method is used to account for the angular distribution of the Ξ . The uncertainty of the parameters used introduce 4% and 5% differences in efficiencies of the χ_{c1} and χ_{c2} channels, respectively, which are taken as the systematic error for the uncertainty of the Ξ angular distribution.
- In the analysis of $\chi_{cJ} \rightarrow \Lambda\bar{\Lambda}\pi^+\pi^-$, the $\Xi^-\bar{\Xi}^+$ intermediate state is excluded, and no significant signals for decays $\chi_{cJ} \rightarrow \Sigma^+(1385)\bar{\Sigma}^-(1385), \Lambda(1405)\bar{\Lambda}(1405)$ are observed. The intermediate state corrections to the detection efficiency are evaluated by considering only the observable decay $\chi_{cJ} \rightarrow \Sigma^-(1385)\bar{\Lambda}\pi^+ + c.c.$. The branching fractions are roughly estimated using data. The efficiency differences are evaluated by:

$$\frac{\delta\epsilon}{\epsilon_1} = \frac{|\epsilon_1 - \epsilon_2|}{\epsilon_1} \frac{B(\chi_{cJ} \rightarrow \Sigma^-(1385)\bar{\Lambda}\pi^+ + c.c.)B(\Sigma^- \rightarrow \Lambda\pi^-)}{B(\chi_{cJ} \rightarrow \Sigma^-(1385)\bar{\Lambda}\pi^+ + c.c.)B(\Sigma^- \rightarrow \Lambda\pi^-) + B(\chi_{cJ} \rightarrow \Lambda\bar{\Lambda}\pi^+\pi^-)},$$

where ϵ_1 and ϵ_2 are the detection efficiencies for $\psi(2S)$ radiative decays via $\chi_{cJ} \rightarrow \Lambda\bar{\Lambda}\pi^+\pi^-$ and $\chi_{cJ} \rightarrow \Sigma^-(1385)\bar{\Lambda}\pi^+ + c.c., \Sigma(1385) \rightarrow \Lambda\pi$, respectively. We obtain the efficiency difference $\delta\epsilon/\epsilon_1 = 7.1\%, 6.0\%$, and 2.6% for decays of χ_{c0}, χ_{c1} , and χ_{c2} , respectively, which is treated as one of the systematic errors. Total systematic errors are given in Table IV.

TABLE IV: Summary of systematic errors (%).

Source	$\chi_{cJ} \rightarrow \Xi^- \bar{\Xi}^+$			$\chi_{cJ} \rightarrow \Lambda \bar{\Lambda} \pi^+ \pi^-$			$\chi_{cJ} \rightarrow K_S^0 K_S^0 p \bar{p}$		
	χ_{c0}	χ_{c1}	χ_{c2}	χ_{c0}	χ_{c1}	χ_{c2}	χ_{c0}	χ_{c1}	χ_{c2}
MDC track	12.0	12.0	12.0	12.0	12.0	12.0	12.0	12.0	12.0
Photon efficiency	2.0	2.0	2.0	2.0	2.0	2.0	2.0	2.0	2.0
4C-fit	4.0	4.0	4.0	4.0	4.0	4.0	4.0	4.0	4.0
Number of $\psi(2S)$	4.0	4.0	4.0	4.0	4.0	4.0	4.0	4.0	4.0
$p\bar{p}$ particle ID	5.6	5.6	5.6	5.6	5.6	5.6	5.6	5.6	5.6
$B(\Lambda \rightarrow p\pi)$	0.8	0.8	0.8	0.8	0.8	0.8	0.8	0.8	0.8
$B(\psi(2S) \rightarrow \gamma\chi_{cJ})$	5.1	6.4	6.7	5.1	6.4	6.7	5.1	6.4	6.7
Background uncertainty	5.0	5.0	5.0	5.3	3.6	2.9	4.0	4.0	4.0
MC statistics	2.0	1.9	2.1	3.5	3.0	3.0	5.0	5.0	5.0
Angular distribution of $\Xi^- \bar{\Xi}^+$	-	4.0	5.0	-	-	-	-	-	-
Intermediate state $\Sigma(1385)$	-	-	-	7.1	6.0	2.6	-	-	-
Total	16.3	17.2	17.6	18.1	17.6	16.7	16.7	17.1	17.3

VII. RESULTS AND DISCUSSION

Using the 14×10^6 $\psi(2S)$ events accumulated at BESII, the analysis of $\chi_{cJ} \rightarrow \Xi^- \bar{\Xi}^+$, $\Lambda \bar{\Lambda} \pi^+ \pi^-$, $K_S^0 K_S^0 p \bar{p}$ is carried out. The measured branching fractions or upper limits are summarized in Table V, along with some theoretical predictions. Theoretically, the quark creation model (QCM) predicts $B(\chi_{c0} \rightarrow \Xi^- \bar{\Xi}^+) = (2.3 \pm 0.7) \times 10^{-4}$, which is consistent with the experimental value within 1σ . For χ_{c1} and χ_{c2} decays into $\Xi^- \bar{\Xi}^+$, the measured upper limits cover both the COM and QCM predictions.

Within 1.8σ the branching fraction of $\chi_{c0} \rightarrow \Xi^- \bar{\Xi}^+$ does not vanish. For further testing of the violation of the HSR in this decay, higher accuracy measurements are required.

TABLE V: The comparison of the branching fractions or upper limits for $\chi_{cJ} \rightarrow \Xi^- \bar{\Xi}^+$, $\Lambda \bar{\Lambda} \pi^+ \pi^-$, and $K_S^0 K_S^0 p \bar{p}$ between experimental values and theoretical predictions. The COM predictions are from Ref. [17], and the quark creation model (QCM) predictions are from Ref. [18].

Decay modes	Branching ratios	Theoretical predictions	
		COM	QCM
$\chi_{c0} \rightarrow \Xi^- \bar{\Xi}^+$	$(5.3 \pm 2.7 \pm 0.9) \times 10^{-4}$ or $< 10.3 \times 10^{-4}$ (90% C.L.)	—	$(2.3 \pm 0.7) \times 10^{-4}$
$\chi_{c1} \rightarrow \Xi^- \bar{\Xi}^+$	$< 3.4 \times 10^{-4}$ (90% C.L.)	2.4×10^{-5}	—
$\chi_{c2} \rightarrow \Xi^- \bar{\Xi}^+$	$< 3.7 \times 10^{-4}$ (90% C.L.)	3.4×10^{-5}	$(4.8 \pm 2.1) \times 10^{-5}$
$\chi_{c0} \rightarrow \Lambda \bar{\Lambda} \pi^+ \pi^-$	$(2.0 \pm 1.1 \pm 0.4) \times 10^{-3}$ (2.5σ) or $< 4.0 \times 10^{-3}$ (90% C.L.)	—	—
$\chi_{c1} \rightarrow \Lambda \bar{\Lambda} \pi^+ \pi^-$	$< 1.5 \times 10^{-3}$ (90% C.L.)	—	—
$\chi_{c2} \rightarrow \Lambda \bar{\Lambda} \pi^+ \pi^-$	$(1.8 \pm 1.0 \pm 0.3) \times 10^{-3}$ (2.5σ) or $< 3.5 \times 10^{-3}$ (90% C.L.)	—	—
$\chi_{c0} \rightarrow K_S^0 K_S^0 p \bar{p}$	$< 8.8 \times 10^{-4}$ (90% C.L.)	—	—
$\chi_{c1} \rightarrow K_S^0 K_S^0 p \bar{p}$	$< 4.5 \times 10^{-4}$ (90% C.L.)	—	—
$\chi_{c2} \rightarrow K_S^0 K_S^0 p \bar{p}$	$< 7.9 \times 10^{-4}$ (90% C.L.)	—	—

VIII. ACKNOWLEDGMENT

The BES collaboration thanks the staff of BEPC for their hard efforts. This work is supported in part by the National Natural Science Foundation of China under contracts Nos. 10491300, 10225524, 10225525, 10425523, the Chinese Academy of Sciences under contract No. KJ 95T-03, the 100 Talents Program of CAS under Contract Nos. U-11, U-24, U-25, and the Knowledge Innovation Project of CAS under Contract Nos. U-602,

U-34 (IHEP), the National Natural Science Foundation of China under Contract No. 10225522 (Tsinghua University), and the Department of Energy under Contract No.DE-FG02-04ER41291 (U Hawaii).

- [1] G. D. Bodwin, E. Braaten, and G. P. Lepage, Phys. Rev. D **51**, 1129 (1995).
- [2] M. Ablikim, *et al.*, (BES Collab.) Phys. Lett. B **630**, 21 (2005);
M. Ablikim, *et al.*, (BES Collab.) Phys. Rev. D **72**, 092002 (2005).
- [3] J. Z. Bai, *et al.*, (BES Collab.) Phys. Rev. D **67**, 032004 (2003);
J. Z. Bai, *et al.*, (BES Collab.) Phys. Rev. D **67**, 112001 (2003);
J. Z. Bai, *et al.*, (BES Collab.) Phys. Rev. D **60**, 072001 (1999);
J. Z. Bai, *et al.*, (BES Collab.) Phys. Rev. Lett. **81**, 3091 (1998).
- [4] S. J. Brodsky, G. P. Lepage, Phys. Rev. D **24**, 2848 (1981).
- [5] S. P. Chi, *et al.*, HEP & NP, **28**, 1135 (2004).
- [6] J. Z. Bai, *et al.*, (BES Collab.) Nucl. Instru. Meth. A **344**, 319 (1994).
- [7] J. Z. Bai, *et al.*, (BES Collab.) Nucl. Instru. Meth. A **458**, 627 (2001).
- [8] M. Ablikim, *et al.*, (BES Collab.) Nucl. Instrum. Meth. A **552**, 344 (2005).
- [9] G. Karl, *et al.*, Phys. Rev. D **13**, 1203 (1976);
L. S. Brown, R. N. Cahn, Phys. Rev. D **13**, 3161 (1976).
- [10] Ping R. G., Yuan C. Z., Commun. Theor. Phys. (Beijing) **44**, 1050 (2005);
Ping Rong-Gang and Du Shu-Xian, Chin. Phys. Lett. **22**, 1309 (2005).
- [11] T. K. Pedlar, *et al.*, (CLEO Collaboration), Phys. Rev. D **72**, 051108 (2005).
- [12] J. Conrad, *et al.*, Phys. Rev. D **67**, 012002 (2003).
- [13] S. B. Athar, *et al.* Phys. Rev. D **70**, 112002 (2004).
- [14] M. Ablikim, *et al.*, (BES Collab.) arXiv:hep-ex/0512025.
- [15] M. Ablikim, *et al.*, (BES Collab.) Nucl. Instru. Meth. A **552**, 344 (2005).
- [16] J. Z. Bai, *et al.*, (BES Collab.) Phys. Rev. D **69**, 072001 (2004).
- [17] S. M. H. Wong, Eur. Phys. J C **14**, 643 (2000).
- [18] R. G. Ping, B. S. Zou, and H. C. Chiang, Eur. Phys. J. A **23**, 129 (2005).